

Anion Substitution in $\text{Ca}(\text{BH}_4)_2\text{--CaI}_2$: Synthesis, Structure and Stability of Three New Compounds

Line H. Rude,[†] Yaroslav Filinchuk,^{*,†,‡,§} Magnus H. Sørby,^{||} Bjørn C. Hauback,^{||} Flemming Besenbacher,[⊥] and Torben R. Jensen^{*,†}

[†]Center for Materials Crystallography (CMC), Interdisciplinary Nanoscience Center (iNANO), and Department of Chemistry, Aarhus University, Langelandsgade 140, DK-8000 Århus C, Denmark

[‡]Swiss–Norwegian Beam Lines at ESRF, BP-220, 38043 Grenoble, France

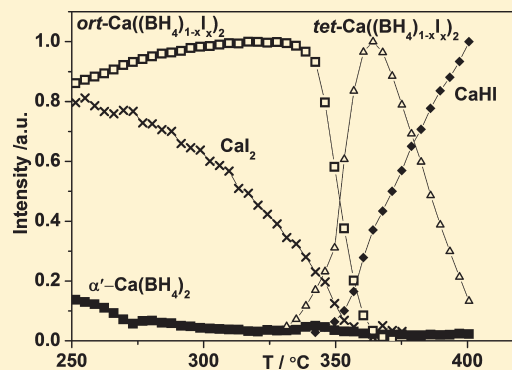
[§]Institute of Condensed Matter and Nanosciences, Université Catholique de Louvain, place L. Pasteur 1, B-1348 Louvain-la-Neuve, Belgium

^{||}Institute for Energy Technology, P.O. Box 40 Kjeller, NO-2027, Norway

[⊥]Interdisciplinary Nanoscience Center (iNANO) and Department of Physics and Astronomy, Aarhus University, DK-8000 Århus C, Denmark

S Supporting Information

ABSTRACT: The substitution of the complex borohydride anion BH_4^- in calcium borohydride by the larger iodide anion I^- is explored in order to tailor the hydrogen storage properties. Three new compounds are identified in the $\text{Ca}(\text{BH}_4)_2\text{--CaI}_2$ system and are structurally characterized using the Rietveld method and synchrotron radiation powder X-ray diffraction (SR-PXD) data. Calcium borohydride readily dissolves in the trigonal calcium iodide structure during ball milling, forming a solid solution $\text{Ca}((\text{BH}_4)_{1-x}\text{I}_x)_2$ with a CaI_2 -type structure and an anisotropically contracted trigonal unit cell, $a = 4.311(1)$ and $c = 6.867(2)$ Å for $x \sim 0.3$ ($T = 28$ °C), space group $P\bar{3}m1$. The trigonal *tri*- $\text{Ca}((\text{BH}_4)_{0.70}\text{I}_{0.30})_2$ transforms at ~ 180 °C to an orthorhombic phase of similar composition, *ort*- $\text{Ca}((\text{BH}_4)_{0.64}\text{I}_{0.36})_2$, with a CaCl_2 -type structure (a distorted β - $\text{Ca}(\text{BH}_4)_2$ type structure) and cell parameters $a = 7.271(2)$, $b = 7.042(1)$, and $c = 4.4601(7)$ Å ($T = 322$ °C), space group $Pnmm$. Further heating of the CaCl_2 -type compound to ~ 330 °C leads to a transition to a tetragonal phase with cell parameters $a = 4.1062(2)$ and $c = 24.822(2)$ Å ($T = 340$ °C, $x \sim 0.62$), space group $I4mm$. This iodide-rich compound *tet*- $\text{Ca}((\text{BH}_4)_{0.38}\text{I}_{0.62})_2$ has a new structure type. The tetragonal phase finally decomposes to CaHI and CaB_6 at $T > 345$ °C. All three novel compounds found in the $\text{Ca}(\text{BH}_4)_2\text{--CaI}_2$ system are stable at room temperature. The anion substitution ultimately changes the decomposition reaction pathway in which hydrogen is released from the tetragonal $\text{Ca}((\text{BH}_4)_{1-x}\text{I}_x)_2$ via CaHI , but unfortunately the temperature of hydrogen release is still fairly high and similar to that for $\text{Ca}(\text{BH}_4)_2$.



1. INTRODUCTION

Renewable energy sources are an environmentally friendly, inexhaustible alternative to fossil fuels, but their utilization is hampered since the energy production generally fluctuates in time and is nonuniformly distributed geographically. The solution should be a safe, cheap, and efficient energy carrier, and hydrogen is a worldwide target receiving increasing political and scientific interest.¹ The characteristics of the ideal hydrogen storage material for mobile applications are high gravimetric and volumetric hydrogen content, the ability to store hydrogen reversibly with fast hydrogen release and uptake kinetics at moderate temperatures, low heat exchange, and preparation from abundant, inexpensive, and robust materials.^{2–4} At present, no single material fulfills all these requirements.^{5–7}

Light metal borohydrides currently receive considerable interest due to their high gravimetric hydrogen contents, e.g., 18.5 wt % for LiBH_4 .⁸ Unfortunately, the utilization of borohydrides for practical applications is often hampered by limited reversibility, unfavorable kinetics, and thermodynamics.^{6,8} Several novel materials have recently been synthesized, e.g., $\text{LiSc}(\text{BH}_4)_4$, $\text{NaSc}(\text{BH}_4)_4$, and $\text{KSc}(\text{BH}_4)_4$ with the complex anion $[\text{Sc}(\text{BH}_4)_4]^-$,^{9–12} $\text{LiZn}_2(\text{BH}_4)_5$, and $\text{NaZn}_2(\text{BH}_4)_5$ with interpenetrated networks, $\text{NaZn}(\text{BH}_4)_3$ ¹³ containing polymeric anions, and $\text{KZn}(\text{BH}_4)\text{Cl}_2$ ¹⁴ with heteroleptic composite anions.

Received: December 2, 2010

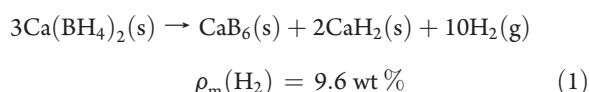
Revised: March 10, 2011

Published: March 29, 2011

These compounds release hydrogen at low temperatures but, in some cases, irreversibly parallel with release of borane gases.¹⁵ This was also observed, although in small amounts, for the more stable ionic borohydrides, e.g., LiBH₄.¹⁶ Bimetallic borohydrides based on the early *d*-block metals and alkali metals, e.g., Sc and Y, clearly have the ability to form stable boron compounds in the solid state, i.e., avoiding the release of borane gases.^{9–12,17–19} Metal borohydrides may also crystallize with partly open structures as observed for Mn(BH₄)₂ and α-Mg(BH₄)₂, which reveal a large structural flexibility for the borohydride materials.^{8,20,21} The properties of known borohydrides may be improved by chemical reactions as realized in reactive hydride composites (RHC), which have the weighted average hydrogen storage capacity as compared to the individual components but may have significantly improved thermodynamic properties as observed for the 2LiBH₄–MgH₂ system.^{22–26} Another approach is anion substitution, which may modify the physical properties of the hydrogen storage material. Theoretical calculations suggest that the substitution of the hydride ion with the more electronegative fluorine ion, i.e., H[−] → F[−], will significantly alter the hydrogen release and uptake properties for the BH₄[−] ion, e.g., in LiBH₄.²⁷ Fluorine substitution has been performed experimentally in aluminum-based alanates, e.g., NaAlH₄,^{28–32} resulting in a destabilization of the material. The heavier halides readily substitute in borohydrides and form solid–solution or stoichiometric compounds, e.g., Cl[−], Br[−], or I[−] can substitute for BH₄[−] in LiBH₄ or Ca(BH₄)₂.^{33–36} By the choice of anion species and the extent of the substitution, it may be possible to modify the conditions for hydrogen uptake and release. Furthermore, anion-substituted borohydrides have significantly improved lithium ion conduction properties.³³

Calcium borohydride, Ca(BH₄)₂, has a high theoretical hydrogen content calculated both gravimetrically, ρ_m = 11.6 wt % H₂, and volumetrically, ρ_v = 108 g H₂/L, and receives increasing interest for utilization as a possible hydrogen storage material.^{37–39} Calcium borohydride exhibits interesting structural chemistry with at least four known polymorphs denoted α-, β-, γ- and α'-Ca(BH₄)₂,^{8,38,40–45} where up to three polymorphs α-, β- and γ-Ca(BH₄)₂ may coexist under ambient conditions. The stable room temperature (RT) polymorph is orthorhombic α-Ca(BH₄)₂ with space group symmetry *F2dd* (no. 43).⁴⁰ A transformation to the high-temperature β-Ca(BH₄)₂ phase occurs at *T* > 176 °C. Different space group symmetries have been suggested for the β-phase, *P4₂/m* (no. 84),^{41,46} *P4₂nm* (no. 102), and *P4* (no. 81),⁴⁰ but all structural models are similar. β-Ca(BH₄)₂ is metastable at RT and slowly transforms to the α-phase upon cooling.^{40,47} The orthorhombic γ-Ca(BH₄)₂ with the space group symmetry *Pbca* (no. 61)^{44,48} transforms to β-Ca(BH₄)₂ at 290 °C. A second-order phase transition from α- to the tetragonal α'-Ca(BH₄)₂, space group *I4₂d* (no. 122), can be observed at 222 °C.⁴⁰

Calcium borohydride decomposes in the temperature range from 360 to 500 °C, releasing 9.6 wt % hydrogen via reaction 1.^{37,38,42,48,49}



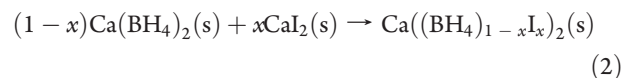
The reaction proceeds in several steps via an intermediate phase identified as CaB₂H_x.⁴⁹ Partial rehydrogenation has been demonstrated at *p*(H₂) = 90 bar and at 350 to 420 °C using additives.^{39,50}

Table 1. List of Investigated Samples^a

notation	materials	molar ratio	<i>n</i> (CaI ₂)/ <i>n</i> (total)	preparation
R1	α- and β-Ca(BH ₄) ₂		0	TT ^b
R2	α-Ca(BH ₄) ₂		0	TT ^b and BM
S1	Ca(BH ₄) ₂ + CaI ₂	1:0.22	0.18	BM
S2	Ca(BH ₄) ₂ + CaI ₂	1:0.42	0.29	BM
S3	Ca(BH ₄) ₂ + CaI ₂	1:0.42	0.29	HM
S4	Ca(BH ₄) ₂ + CaI ₂	1:0.86	0.46	BM

^aThe composition of the samples is given as the molar ratios and the molar fractions, *n*(CaI₂)/*n*(total). The preparation methods are either ball milling (BM), hand-mixing in a mortar (HM) or thermal treatment (TT) in argon atmosphere. ^b170 °C/24 h cooled naturally in air to RT.

The high decomposition temperature makes calcium borohydride unsuitable for practical hydrogen storage applications,³⁸ and it is therefore tempting to modify the thermodynamics and kinetics of hydrogen release and uptake using partial anion substitution. This has prompted us to study the substitution of the complex anion BH₄[−] by the larger iodide anion, I[−], as described in reaction scheme 2,



Here we present synthesis, crystal structures, and thermal transformation of three new iodide-substituted calcium borohydrides investigated by in situ synchrotron radiation powder X-ray diffraction along with an investigation of their hydrogen storage properties.

2. EXPERIMENTAL SECTION

2.1. Sample Preparation. Calcium borohydride was prepared from commercially available Ca(BH₄)₂·2THF (Aldrich) by desolvating in vacuum (*p* ~ 10^{−1} mbar) for 24 h at 170 °C, denoted TT (thermal treatment) in Table 1. The obtained product, denoted R1, was a mixture of α- and β-Ca(BH₄)₂. A sample of α-Ca(BH₄)₂, denoted R2, was produced by ball milling (BM) a fraction of R1 for 2 h at 250 rpm (2 min, 2 min break, 60 repetitions) and with a sample to ball ratio of approximately 1: 30. The vial was sealed with a lid and a Teflon O-ring under purified argon atmosphere.

Sample R1, α- and β-Ca(BH₄)₂ was mixed with CaI₂ (Aldrich, 99.999%) in molar ratios of 1:0.22, producing a sample denoted S1, 1:0.42 (S2), or 1:0.86 (S4) and ball milled using the procedure described above. A similar sample in the molar ratio 1:0.42 (S3) was hand-mixed (HM) for 10 min in an agate mortar. The investigated samples are listed in Table 1. All handling and manipulation of the chemicals and sample preparations were performed in an argon-filled glovebox with circulation purifier, *p*(O₂, H₂O) < 0.5 ppm.

2.2. In Situ Synchrotron Radiation Powder X-ray Diffraction. In situ synchrotron radiation powder X-ray diffraction (SR-PXD) data for samples S1, S2, S3, and S4 were measured at the beamline BM01A at the Swiss–Norwegian Beamlines (SNBL), European Synchrotron Radiation Facility (ESRF), Grenoble, France, using a MAR345 image plate detector. The samples were mounted in glass capillaries sealed with a composite adhesive in an argon atmosphere (1 bar) to prevent contact with air.⁵¹ The data were collected at a sample-to-detector distance of 275 mm (S1, S2, and S3) and 200 mm (S4), and the capillaries

Table 2. The Crystal System, Unit Cell Parameters and Space Group for the Three New Compounds Found in This Study Compared to Selected Known Compounds^a

structure	crystal system	space group	<i>a</i> /Å	<i>b</i> /Å	<i>c</i> /Å	<i>V</i> /Å ³	<i>T</i> /°C
α-Ca(BH ₄) ₂ ⁴⁰	orthorhombic	<i>F2dd</i>	8.7759(3)	13.0234(4)	7.4132(2)	847.27	−183
β-Ca(BH ₄) ₂ ⁴⁰	tetragonal	<i>P4₂nm</i> or <i>P4̄</i>	6.91894(11)		4.34711(12)	208.10	222
β-Ca(BH ₄) ₂ ⁴¹	tetragonal	<i>P4₂/m</i>	6.9468(1)		4.3661(1)	210.70	207
CaI ₂ ⁵⁷	trigonal	<i>P3̄m1</i>	4.49(2)		6.975(30)	121.78	RT
CaCl ₂ ⁵⁹	orthorhombic	<i>Pnmm</i>	6.24	6.43	4.2	168.52	RT
CaHI ⁵⁸	tetragonal	<i>P4/nmm</i>	4.071		8.941	148.18	RT
<i>tri</i> -Ca((BH ₄) _{0.70} I _{0.30}) ₂ ^b	trigonal	<i>P3̄m1</i>	4.3107(11)		6.8669(19)	110.51	28
<i>ort</i> -Ca((BH ₄) _{0.64} I _{0.36}) ₂ ^b	orthorhombic	<i>Pnmm</i>	7.2713(15)	7.04182(12)	4.4600(6)	228.37	322
<i>tet</i> -Ca((BH ₄) _{0.38} I _{0.62}) ₂ ^b	tetragonal	<i>I4mm</i>	4.1067(2)		24.821(2)	418.51	340

^aThe X-ray data collection temperature is given for comparison. ^bThis work.

were rotated 20° during the data collection. The X-ray exposure time for each powder pattern was 20 s using selected wavelengths of $\lambda = 0.703511$ Å (S1 and S3), $\lambda = 0.6548$ Å (S2), and $\lambda = 0.721082$ Å (S4). The wavelength and the detector geometry were calibrated using an external standard, LaB₆. Decomposition reactions were investigated in the temperature range from RT to 360 °C for samples S1 and S3, and from RT to 400 °C for samples S2 and S4 using heating rates of 3, 4, 2, and 2 °C/min, respectively.

The data were integrated using the Fit2D program,⁵² and uncertainties for the integrated intensities were calculated using each 2θ -point, taking the geometry of the detector into consideration.⁵³ The relative amounts of the different phases in the investigated samples were estimated by integrating the intensity of selected Bragg reflections applying a Gaussian fit and subtracting the background intensity by use of a linear interpolation. The integrated intensities are normalized and shown as a function of temperature (The intensity, $\alpha(t) = I_i(t)/I_{i,max}$ for the compound *i* at the time *t*). The unit cell parameters were determined with the DICVOL2004 software,⁵⁴ and structural models were obtained using direct space algorithms implemented in the program FOX.⁵⁵ The structural models were refined with the Rietveld methods in the FullProf suite.⁵⁶ The sequential refinement of the in situ SR-PXD data was performed to follow the change in composition and unit cell volumes. Previously published structural parameters were used as an initial input for the Rietveld refinements when available.^{40,57–59}

2.3. Thermal Analysis. Differential scanning calorimetry (DSC) and thermogravimetric analysis (TGA) were performed simultaneously with a Netzsch STA449C Jupiter instrument at heating and cooling rates of 10.0 °C/min in a flow of He (50 mL/min) for samples R1, S1, and S2. Prior to the experiment, the samples were heated to 300 °C and cooled to RT three times in order to investigate the dynamic properties of the substitution process. The fourth heating was continued to 550 °C to determine the hydrogen release. The samples were mounted in Al₂O₃ crucibles with tiny holes in the lid to prevent increase in pressure during desorption of gases.

Sieverts measurements were recorded with a PCTpro 2000 instrument from Hy-Energy.⁶⁰ The samples were loaded in an autoclave and sealed in argon atmosphere. Temperature–pressure desorption (TPD) experiments were performed in the temperature range from RT to 550 °C with a heating rate of 0.5 °C/min in vacuum. Hydrogen absorption data were measured in the temperature range RT to 350 °C (20 °C/min)

followed by 10 h at a fixed temperature of 350 °C. A hydrogen pressure of ca. 100 bar was initially applied.

3. RESULTS AND DISCUSSION

To study the substitution of CaI₂ into Ca(BH₄)₂, four different samples (S1–4, see Table 1) were prepared and characterized by in situ SR-PXD at variable temperatures to probe the mechanism for the substitution and the structural chemistry of the different phases. Three new compounds were found in the Ca(BH₄)₂–CaI₂ system and structurally characterized as summarized in Table 2.

3.1. Structural Investigation of Three New Compounds Observed in the Ca(BH₄)₂–CaI₂ System. A set of relatively broad Bragg peaks are observed at RT for all ball-milled Ca(BH₄)₂–CaI₂ samples (S1, S2, S4). These reflections were indexed with a trigonal unit cell, similar to the one for the CaI₂ structure. Global structural optimization using the program FOX and space group *P3̄m1* and followed by Rietveld refinement showed that the Ca(BH₄)₂–CaI₂ (0.71:0.29, S2) mixture became a single phase with a CaI₂-type structure and a refined iodide concentration of 0.30(2), i.e., *tri*-Ca((BH₄)_{0.70}I_{0.30})₂, in agreement with the nominal composition. The Rietveld refinement converged at $R_B = 4.18\%$ and $R_{wp} = 11.6\%$ (conventional indexes, these are more correct values as the fit to the background is not included), and $R_{wp} = 3.21\%$ (not corrected for background). The observed and calculated PXD profiles are shown in Figure 1, and the structure of the trigonal solid solution is illustrated in Figure 2. Atomic coordinates and selected bond lengths are given in the Supporting Information (see Tables s1 and s2).

Calcium cations in the trigonal, *tri*-Ca((BH₄)_{0.70}I_{0.30})₂, structure are octahedrally coordinated by six anions (I[−] or BH₄[−]), CN(Ca) = 6. Each anion is coordinated to three Ca atoms (CN = 3) situated in the base of a trigonal pyramid. On the other side, the anion is pointing to the middle of the triangle formed by iodide/BH₄[−] units of the neighboring layer (see Figure 2) and the anion–anion distances are 4.197(6) Å. The cation–anion distances in the BH₄-substituted compound are slightly shorter than in CaI₂, i.e., 3.039(3) and 3.124(6) Å, respectively.⁵⁷ The unit cell volume per formula unit, *V*/*Z*, clearly decreases as a consequence of dissolution of Ca(BH₄)₂ in CaI₂, i.e., from 121.8 to 110.5 Å³ for CaI₂ and Ca((BH₄)_{0.70}I_{0.30})₂, respectively, which correlates with the size of the respective anions.⁶¹

Further heating of the trigonal solid solution, *tri*-Ca((BH₄)_{0.70}I_{0.30})₂ obtained from sample S2 leads to the formation of a new compound observed at ~180 °C. The new set of Bragg

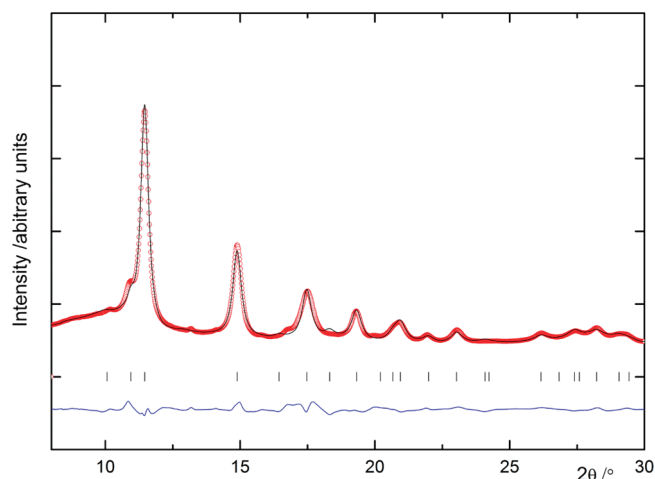


Figure 1. Rietveld refinement profile of a new CaI_2 -type trigonal compound, $\text{tri-Ca}((\text{BH}_4)_{0.70}\text{I}_{0.30})_2$, space group $P\bar{3}m1$, formed by ball milling sample S2. The red circles depict the observed data, and the black line shows the calculated fit. The difference plot is shown in blue. The data was collected at 28 °C, using $\lambda = 0.6548 \text{ \AA}$.

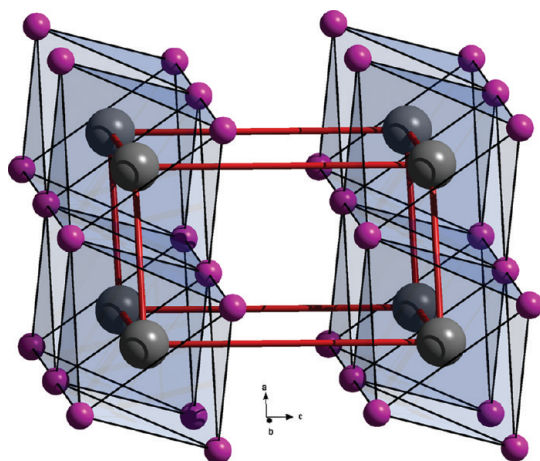


Figure 2. Crystal structure of a new CaI_2 -type trigonal compound, $\text{tri-Ca}((\text{BH}_4)_{0.70}\text{I}_{0.30})_2$. The calcium atoms are shown in gray, and I^- and BH_4^- , obtaining the same positions, are shown as purple spheres.

reflections was indexed by an orthorhombic unit cell, and a structural model was created in the space group $Pnmm$ using FOX.⁵⁵ The resulting structural model is a CaCl_2 -type structure, with the site of the anion statistically occupied by iodide ions and borohydride complexes. The refined composition $\text{ort-Ca}((\text{BH}_4)_{0.64}\text{I}_{0.36})_2$ of the single-phase sample ($T = 322 \text{ °C}$, S2) is similar to the composition of the trigonal phase. Rietveld refinement of the structural model converged at $R_B = 7.69\%$ and $R_{\text{wp}} = 11.3\%$ (conventional indexes) and $R_{\text{wp}} = 2.91\%$ (not corrected for background). The observed and calculated profiles are shown in Figure 3, and the structure of the orthorhombic phase is illustrated in Figure 4. Atomic coordinates and selected bond lengths are given in the Supporting Information (see Tables s3 and s4). The orthorhombic phase is stable upon cooling to room temperature.

Calcium cations in the orthorhombic solid solution have octahedral coordination (CN = 6) to six BH_4^- or I^- ions. However,

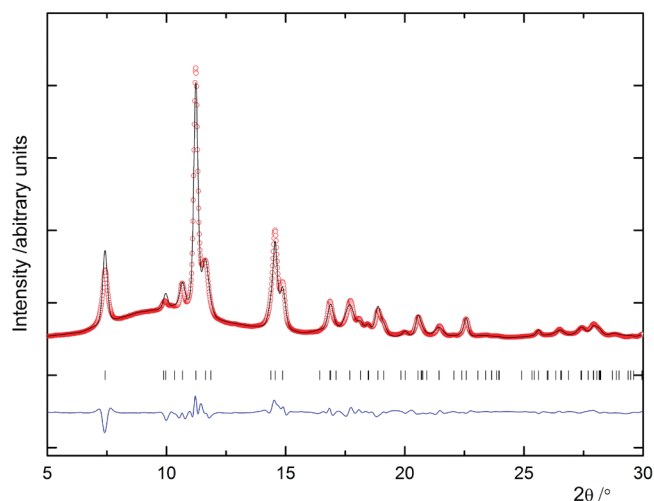


Figure 3. Rietveld refinement profile of a new CaCl_2 -type orthorhombic structure, $\text{ort-Ca}((\text{BH}_4)_{0.64}\text{I}_{0.36})_2$, space group $Pnmm$, formed by heating sample S2 to 322 °C. The red circles depict the observed data, and the black line shows the calculated fit. The difference plot is shown in blue. The data was collected at 322 °C, using $\lambda = 0.6548 \text{ \AA}$.

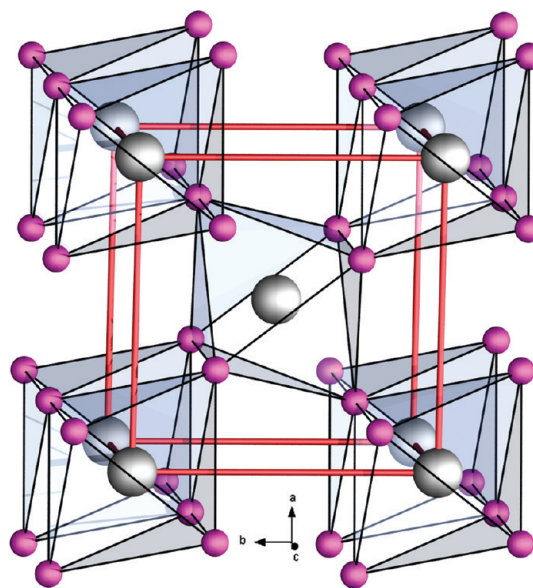


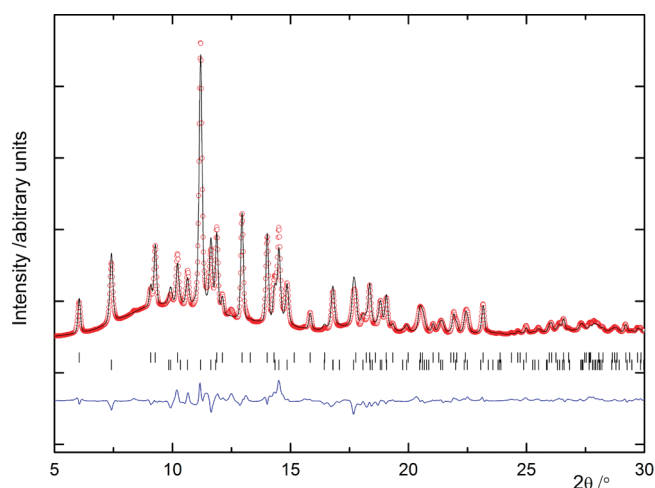
Figure 4. Crystal structure of a new CaCl_2 -type orthorhombic structure, $\text{ort-Ca}((\text{BH}_4)_{0.64}\text{I}_{0.36})_2$. The calcium atoms are shown in gray, and I^- and BH_4^- , occupying the same position, are marked as purple spheres.

the anion sites have a different environment, namely trigonal-planar (CN = 3) as compared to the trigonal pyramidal coordination in the trigonal phase. The resulting structure is not layered, but polymeric in all three dimensions (see Figure 4). The Ca–anion distance is 2.967(3) and 3.026(2) Å at RT, which is significantly longer than the Ca–Cl distances in CaCl_2 (2.70(5) to 2.76(3) Å at RT) due to the larger radius of I^- and BH_4^- ions as compared to Cl^- ions. The shortest anion–anion distances are 4.166(5) and 3.59(7) Å in the orthorhombic solid solution and CaCl_2 , respectively (see Table 3).

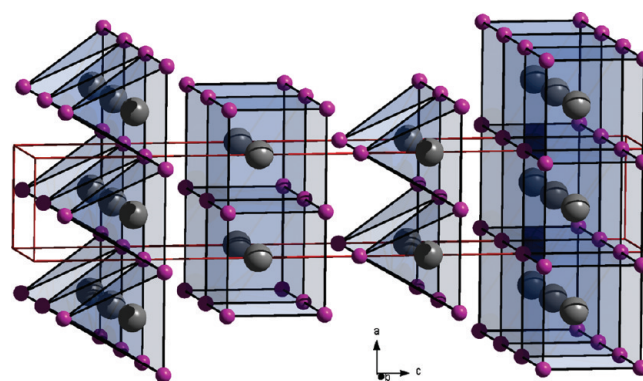
The symmetry of the orthorhombic phase shows an interesting aspect with respect to the iodide-free $\beta\text{-Ca}(\text{BH}_4)_2$. Similar to

Table 3. Essential Interatomic Distances Determined from Diffraction Data Measured at Different Temperatures for the Three New Compounds Observed in This Study and for Selected Known Compounds

compound	anion	Ca...anion /Å	shortest anion...anion /Å	T /°C
α -Ca(BH ₄) ₂ ⁴⁰	BH ₄ ⁻	2.816(8)–2.967(8)	3.648(11)	–183
β -Ca(BH ₄) ₂ ⁴⁰	BH ₄ ⁻	2.923(8)–2.939(8)	3.80(2)	32
CaI ₂ ⁵⁷	I ⁻	3.124(6)	4.345(12)	RT
CaCl ₂ ⁵⁹	Cl ⁻	2.70(5)–2.76(3)	3.59(7)	RT
tri-Ca((BH ₄) _{0.70} I _{0.30}) ₂ ^a	I ⁻ /BH ₄ ⁻	3.039(3)	4.197(6)	44
ort-Ca((BH ₄) _{0.64} I _{0.36}) ₂ ^a	I ⁻ /BH ₄ ⁻	3.007(3)–3.057(2)	4.181(4)	322
tet-Ca((BH ₄) _{0.38} I _{0.62}) ₂ ^a	I ⁻ /BH ₄ ⁻	2.79(3)–3.70(4)	3.43(2)	340

^aThis work.**Figure 5.** Rietveld refinement profile of a new tetragonal structure, *tet*-Ca((BH₄)_{0.38}I_{0.62})₂, space group *I4mm*, formed by heating sample **S2** to 340 °C. The sample contains only 20 wt % of this phase and 80 wt % of the orthorhombic *ort*-Ca((BH₄)_{0.61}I_{0.39})₂ CaCl₂-type structure (lower tick marks). The red circles depict the observed data and black line shows the calculated fit. The difference plot is shown in blue. The data was collected at 340 °C using $\lambda = 0.6548$ Å.

CaCl₂, which undergoes a second-order phase transition from a *Pnmm* to a *P4₂/mnm* phase on heating,⁶² the former is a distortion of the latter. The actual symmetry of a number of *Pnmm* structures, known as FeS₂-type structures, can be lower, namely *Pnn2*.⁶³ Therefore, a group–subgroup relation between the *ort*-Ca((BH₄)_{1-x}I_x)₂ (*Pnmm*) and the tetragonal β -Ca(BH₄)₂ phase holds only for one of the three space group symmetries (*P4₂/m*,⁴¹ *P4₂nm* or *P4⁻*)⁴⁰ suggested for the β -Ca(BH₄)₂ structures, i.e. *Pnn2* \leftrightarrow *P4₂nm*. The *P4₂nm* symmetry also corresponds with the observed systematic absences in the diffraction data.⁴⁰ We attempted to refine the orthorhombic Ca((BH₄)_{1-x}I_x)₂ structure in the space group *Pnn2*, but with no obvious improvement of the fit. This argument alone cannot rule out the lower symmetry, since the differentiation between the two space groups from diffraction data was shown to be a challenge,⁶⁴ and the apparent deviation from the centrosymmetric *Pnmm* model appears to be small for other AB₂ systems.⁶³ The BH₄⁻ groups in β -Ca(BH₄)₂ may be intrinsically disordered, similar to the high-temperature hexagonal polymorph of LiBH₄,⁶⁵ which may contribute to the difficulties in theoretical description of the structure using a harmonic approximation⁶⁶ or experimentally using powder diffraction data.^{40,41}

**Figure 6.** Crystal structure of tetragonal, *tet*-Ca((BH₄)_{0.38}I_{0.62})₂. The calcium atoms are shown as gray spheres and the anions are shown as purple spheres. The space group is *I4mm*, and the cell parameters are $a = 4.110$ and $c = 24.845$ Å at $T = 340$ °C.

Further heating of the CaCl₂-type solid solution, *ort*-Ca((BH₄)_{0.64}I_{0.36})₂ (322 °C, **S2**), provides another new powder diffraction profile observed at 335 °C. The new solid solution is observed in a temperature interval from 335 to \sim 400 °C, but already starts to decompose at \sim 345 °C. The highest quality diffraction pattern is collected at 340 °C for a sample (**S2**) containing a mixture of the CaCl₂-type solid solution and the new phase (see Figure 5). This data allows indexing the new set of diffraction peaks with a tetragonal cell, $a = b = 4.1067(2)$ and $c = 24.821(2)$ Å, and was used for structure determination. Systematic absences suggest a body-centered cell, and the global optimization in FOX yielded a reasonable structure in the space group *I4mm*. The presented structural model is only tentative and still needs to be confirmed or revised by other methods. The structure contains two Ca atom sites and four sites occupied by I⁻ and BH₄⁻ anions. Two of them (I1 and I2) appear to be fully occupied by I⁻, and the other two (I3 and I4) appear to be occupied by a statistical mixture of borohydride and iodide anions. The Rietveld refinement converged at $R_B = 8.74\%$ and $R_{wp} = 16.1\%$ (conventional indexes) and $R_{wp} = 3.73\%$ (not corrected for background). The refined composition for the new tetragonal *I4mm* structure is *tet*-Ca((BH₄)_{0.38}I_{0.62})₂ (340 °C, **S2**), and the sample contained only 20 wt % of this phase, and 80 wt % of the *ort*-Ca((BH₄)_{0.61}I_{0.39})₂ (340 °C, **S2**). The observed and calculated profiles are shown in Figure 5, and the structure of the tetragonal phase is illustrated in Figure 6. Atomic coordinates and selected bond lengths are given in the Supporting Information (see Tables s5 and s6).

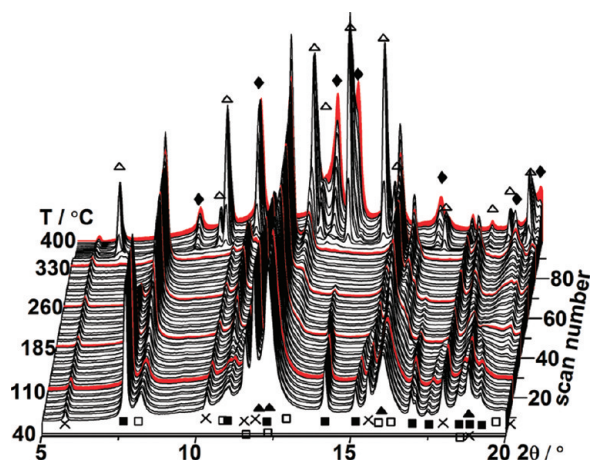


Figure 7. In situ SR-PXD data measured for $\text{Ca}(\text{BH}_4)_2\text{-CaI}_2$ (0.82:0.18, S1) heated from RT to 400 °C (heating rate 2 °C/min, $\lambda = 0.703511$ Å). Symbols: ■ $\alpha\text{-Ca}(\text{BH}_4)_2$ and $\alpha'\text{-Ca}(\text{BH}_4)_2$, × CaI_2 , ▲ $\text{tri-Ca}((\text{BH}_4)_{1-x}\text{I}_x)_2$, □ $\text{ort-Ca}((\text{BH}_4)_{1-x}\text{I}_x)_2$, △ $\text{tet-Ca}((\text{BH}_4)_{1-x}\text{I}_x)_2$, and ◆ CaHI .

The tetragonal $I4mm$ phase has a long c -axis as compared to the cell parameters in the a,b basal plane and to other similar compounds (see Table 2). The structure is relatively rich in iodide and is built of layers similar to the CaI_2 structure. However, the coordination numbers for Ca atoms differ significantly. The Ca1 site has a slightly distorted cubic environment (CN = 8) with Ca–anion distances in the range 3.35(2) to 3.70(4) Å, while the Ca2 site has a tetragonal–pyramidal coordination (CN = 5) with significantly shorter distances of 2.79(3)–3.026(13) Å. As illustrated in Figure 6, the layers of cubic and pyramidal coordination alter along the c -axis, forming the I2...I3 contact of 3.43(2) Å. This distance is somewhat shorter compared to the other distances between the anions, which are closer to the expected values of ~ 4.0 Å. The shortest Ca–anion and anion–anion distances for the new compounds observed in this study and for selected known phases are listed in Table 3.

3.2. In Situ SR-PXD Characterization of the System $\text{Ca}(\text{BH}_4)_2\text{-CaI}_2$. A series of in situ SR-PXD patterns of a ball-milled sample of $\text{Ca}(\text{BH}_4)_2\text{-CaI}_2$ (0.82:0.18, S1) is shown in Figure 7 in the temperature range 44–400 °C (2 °C/min). The first pattern includes Bragg reflections from the reactants α - and β - $\text{Ca}(\text{BH}_4)_2$ and CaI_2 and a number of broad reflections from the trigonal, $\text{tri-Ca}((\text{BH}_4)_{0.61}\text{I}_{0.39})_2$ (44 °C, S1), solid solution. This indicates that calcium borohydride dissolves in the structure of calcium iodide during the mechano-chemical treatment, i.e., ball milling giving a solid solution, $\text{tri-Ca}((\text{BH}_4)_{0.61}\text{I}_{0.39})_2$ isomorphous to CaI_2 . Rietveld refinement of PXD data measured at $T = 44$ °C also indicate that a minor amount of CaI_2 (e.g., up to ca. 5%) may dissolve in $\beta\text{-Ca}(\text{BH}_4)_2$ possibly facilitated by the fact that the solid solution $\text{ort-Ca}((\text{BH}_4)_{1-x}\text{I}_x)_2$ and $\beta\text{-Ca}(\text{BH}_4)_2$ are structurally similar.

Several reactions occur, in some cases simultaneously or as coupled chemical reactions, during heating of the sample as discussed in the following. This is visualized by integrating selected well-resolved reflections from observed phases. The data is shown in Figure 8 as normalized integrated intensities for the temperature range from 250 to 400 °C to obtain an overview of the sample composition as a function of temperature.

The second-order phase transition α - to $\alpha'\text{-Ca}(\text{BH}_4)_2$ is observed in Figure 7 at 222 °C, following an increase in the

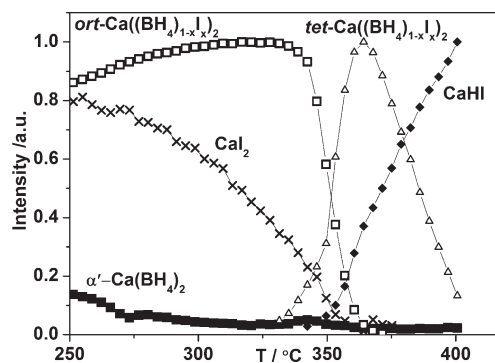


Figure 8. Normalized and integrated intensities for the temperature range 250–400 °C of the in situ SR-PXD data measured for $\text{Ca}(\text{BH}_4)_2\text{-CaI}_2$ (0.82:0.18, S1; see Figure 7). Symbols: ■ $\alpha'\text{-Ca}(\text{BH}_4)_2$, × CaI_2 , □ $\text{ort-Ca}((\text{BH}_4)_{1-x}\text{I}_x)_2$, △ $\text{tet-Ca}((\text{BH}_4)_{1-x}\text{I}_x)_2$, and ◆ CaHI .

a -axis unit cell parameter simultaneously with a decrease in the b -axis parameter over a broad temperature range.⁴⁰ Further heating results in the formation of $\beta\text{-Ca}(\text{BH}_4)_2$ from $\alpha'\text{-Ca}(\text{BH}_4)_2$ and the polymorphic transformations are summarized in the reaction Scheme 3.



The α' -phase is completely transformed to $\beta\text{-Ca}(\text{BH}_4)_2$ at ~ 270 °C. The gradual structural transformation from $\text{tri-Ca}((\text{BH}_4)_{1-x}\text{I}_x)_2$ to the orthorhombic, $\text{ort-Ca}((\text{BH}_4)_{1-x}\text{I}_x)_2$, solid solution is observed in the temperature range 150–313 °C. The refined iodide content of $\text{ort-Ca}((\text{BH}_4)_{0.77}\text{I}_{0.23})_2$ ($T = 313$ °C, S1) is lower than the iodide content in the trigonal phase, indicating that the orthorhombic phase is formed by dissolving $\beta\text{-Ca}(\text{BH}_4)_2$ in the trigonal phase.

However, most diffraction peaks from the tetragonal $\beta\text{-Ca}(\text{BH}_4)_2$ and the $\text{ort-Ca}((\text{BH}_4)_{1-x}\text{I}_x)_2$ coincide, and the two compounds can only be distinguished by differences in the relative Bragg peak intensities and splitting of the reflections. The splitting is due to the expansion of the $\text{ort-Ca}((\text{BH}_4)_{0.77}\text{I}_{0.23})_2$ (313 °C, S1) unit cell by the iodide substitution and a small difference in a and b unit cell parameters.

The PXD patterns at 300 °C contain only diffraction peaks from the $\text{ort-Ca}((\text{BH}_4)_{0.77}\text{I}_{0.23})_2$ (313 °C, S1) and CaI_2 . The intensity of some CaI_2 reflections decreases in the temperature range 250 to ~ 360 °C simultaneously with an increase in the $\text{ort-Ca}((\text{BH}_4)_{0.77}\text{I}_{0.23})_2$ (313 °C, S1), see Figure 8, however no significant change in the composition of $\text{ort-Ca}((\text{BH}_4)_{0.77}\text{I}_{0.23})_2$ (313 °C, S1) was observed by Rietveld refinement of the X-ray data. On the other hand, some Bragg reflections, e.g., peaks at 11.43, 17.82, and 21.24° 2θ , of the CaI_2 phase increase in intensity, which may be due to the formation of an unknown high-temperature polymorph of CaI_2 . This unidentified phase is clearly observed in the hand-mixed sample in the same temperature range. The intensity of the orthorhombic solid solution increases until a rapid transformation at ~ 340 °C to the tetragonal compound, $\text{tet-Ca}((\text{BH}_4)_{0.35}\text{I}_{0.65})_2$ (361 °C, S1) (see Figure 8) with an associated mass loss (as discussed in the following section). The tetragonal phase only exists in a narrow temperature range as the slow decomposition to CaHI and amorphous CaB_6 initiates at 350 °C. The formation of amorphous CaB_6 was observed by solid-state MAS NMR and will be the focus of a future publication. Despite the decomposition of $\text{tet-Ca}((\text{BH}_4)_{1-x}\text{I}_x)_2$, the reflections from this phase are

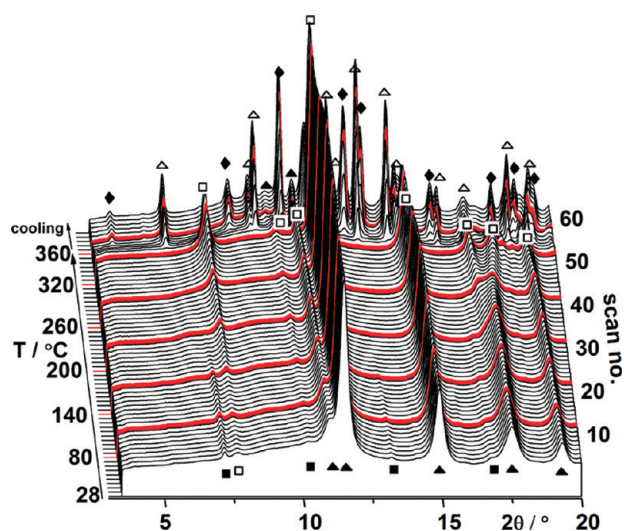


Figure 9. In situ SR-PXD data measured for $\text{Ca}(\text{BH}_4)_2\text{-CaI}_2$ (0.71: 0.29, S2) heated from RT to 360 °C (heating rate 3 °C/min, $\lambda = 0.6548$ Å). Symbols: \blacksquare $\alpha\text{-Ca}(\text{BH}_4)_2$, \blacktriangle $\text{tri-Ca}((\text{BH}_4)_{1-x}\text{I}_x)_2$, \square $\text{ort-Ca}((\text{BH}_4)_{1-x}\text{I}_x)_2$, \triangle $\text{tet-Ca}((\text{BH}_4)_{1-x}\text{I}_x)_2$, and \blacklozenge CaHI.

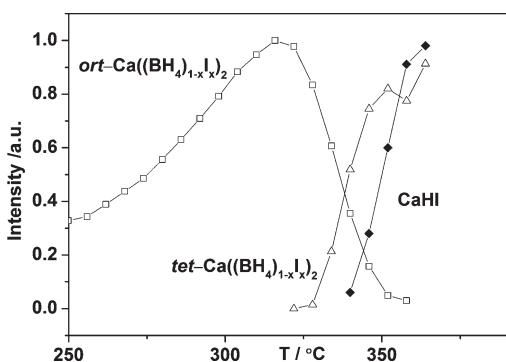


Figure 10. Normalized and integrated intensities for the temperature range 250 to 360 °C of the in situ SR-PXD data measured for $\text{Ca}(\text{BH}_4)_2\text{-CaI}_2$ (0.71: 0.29, S2; see Figure 9). Symbols: \square $\text{ort-Ca}((\text{BH}_4)_{1-x}\text{I}_x)_2$, \triangle $\text{tet-Ca}((\text{BH}_4)_{1-x}\text{I}_x)_2$, and \blacklozenge CaHI.

observed up to a temperature of 400 °C in the last SR-PXD pattern. The amount of $\text{tet-Ca}((\text{BH}_4)_{1-x}\text{I}_x)_2$ is a balance between two chemical reactions, i.e., the transformation from $\text{ort-Ca}((\text{BH}_4)_{1-x}\text{I}_x)_2$ and the decomposition to CaHI and CaB_6 . The largest fraction of $\text{tet-Ca}((\text{BH}_4)_{1-x}\text{I}_x)_2$ is therefore observed at 365 °C (see Figure 8).

The in situ SR-PXD data for $\text{Ca}(\text{BH}_4)_2\text{-CaI}_2$ (0.71: 0.29, S2) heated from RT to 360 °C are shown in Figure 9. The first PXD patterns are dominated by the relatively broad reflections from $\text{tri-Ca}((\text{BH}_4)_{0.70}\text{I}_{0.30})_2$ (RT, S2) and weak reflections from $\alpha\text{-Ca}(\text{BH}_4)_2$. A slow formation of $\text{ort-Ca}((\text{BH}_4)_{1-x}\text{I}_x)_2$ was observed in the temperature range 160–322 °C by decreasing the intensity from the $\alpha\text{-Ca}(\text{BH}_4)_2$ phase and by a gradual splitting of the reflection at $2\theta = 17.5^\circ$. The orthorhombic solid solution transforms to the $\text{tet-Ca}((\text{BH}_4)_{1-x}\text{I}_x)_2$ at 335 °C, which starts to decompose to CaHI and CaB_6 as observed for the sample S1. This is clearly observed in Figure 10, showing the integrated and normalized intensities of the observed phases for the temperature range 250–360 °C.

Table 4. Compositions of the Solid Solutions Found in the Four Investigated Samples S1–S4^a

compound	$x_{\text{S1}} (T/^\circ\text{C})$	$x_{\text{S2}} (T/^\circ\text{C})$	$x_{\text{S3}} (T/^\circ\text{C})$	$x_{\text{S4}} (T/^\circ\text{C})$
$\beta\text{-Ca}((\text{BH}_4)_{1-x}\text{I}_x)_2$	0.05(44)		0.00(44)	
$\text{tri-Ca}((\text{BH}_4)_{1-x}\text{I}_x)_2$	0.39(44)	0.30(28)		$\sim 0.3(26)$
$\text{ort-Ca}((\text{BH}_4)_{1-x}\text{I}_x)_2$	0.23(313)	0.36(32)		
$\text{tet-Ca}((\text{BH}_4)_{1-x}\text{I}_x)_2$	0.65(361)	0.62(34)	0.61(170) ^b	$\sim 0.6(40)$

^a The temperature for the X-ray data collections is given in parentheses. For sample S4 the iodide content is estimated from the volume of the compounds. ^b The compound forms during cooling of the sample.

In order to investigate the influence of the preparation method on the reaction pathway, a sample of $\text{Ca}(\text{BH}_4)_2\text{-CaI}_2$ (0.71: 0.29, S3) was prepared by hand mixing in an agate mortar, and the in situ SR-PXD investigation is shown in the Supporting Information as Figure s1. No reaction between the pure compounds was observed at temperatures below $T < 360$ °C, indicating that the substitution process is mediated by either the shear strain or pressure during ball milling⁶⁷ or by heating to temperatures above 360 °C. The transformation from α - to α' - and further to $\beta\text{-Ca}(\text{BH}_4)_2$ was observed in the temperature range 160 to 290 °C. However, during cooling the formation of the tetragonal solid solution was observed with iodide content similar to what was observed for the samples S1 and S2. Furthermore, at least one unidentified product was observed to form, with peak positions very similar to CaI_2 , indicating that the product is a high-temperature or disordered form of CaI_2 . The integrated and normalized intensities for the temperature range from 100 to 360 °C are shown in the Supporting Information, see Figure s2. As opposed to the other samples, the transformation from α - to $\alpha'\text{-Ca}(\text{BH}_4)_2$ and further to $\beta\text{-Ca}(\text{BH}_4)_2$ is observed as a two-step transformation from α - to $\beta\text{-Ca}(\text{BH}_4)_2$ in Figure s2. A decrease in the diffracted intensity from CaI_2 is observed at 360 °C due to the formation of $\text{tet-Ca}((\text{BH}_4)_{1-x}\text{I}_x)_2$.

To explore the maximum degree of substitution, an iodide-rich sample was prepared (S4). The in situ SR-PXD data measured for the sample $\text{Ca}(\text{BH}_4)_2\text{-CaI}_2$ (0.54: 0.46, S4) heated from RT to 400 °C is shown in the Supporting Information as Figure s3. At RT the sample consists of broad Bragg reflections from a $\text{tri-Ca}((\text{BH}_4)_{1-x}\text{I}_x)_2$ phase, excess of CaI_2 and trace amounts of α - and $\beta\text{-Ca}(\text{BH}_4)_2$. The composition of the trigonal phases cannot be found at RT by Rietveld refinement of the data; however, it can be estimated from the unit cell volume and appears to be similar to what was observed for the samples S1 and S2, $\text{tri-Ca}((\text{BH}_4)_{0.70}\text{I}_{0.30})_2$. The trigonal phase is observed in the temperature range from RT to 400 °C. However, some transformation to the tetragonal phase and the decomposition product CaHI was observed during cooling.

An overview of the compositions of the solid solutions and the temperature for X-ray data collection is presented in Table 4. The temperature region of existence for the observed solid solutions and their compositions is found in the Supporting Information, Table s7.

It is noteworthy that the solid solution occurs with the distorted $\beta\text{-Ca}(\text{BH}_4)_2$, $\text{ort-Ca}((\text{BH}_4)_{1-x}\text{I}_x)_2$ structure. Rietveld refinements reveal that the CaI_2 does not dissolve any $\alpha\text{-Ca}(\text{BH}_4)_2$ upon heating of the ball milled mixtures (samples S1 and S2). Therefore, the α - to $\alpha'\text{-Ca}(\text{BH}_4)_2$ phase transition is observed at similar temperatures as for pure $\alpha\text{-Ca}(\text{BH}_4)_2$ (~ 222 °C) in all the heated $\text{Ca}(\text{BH}_4)_2\text{-CaI}_2$ mixtures.⁴⁰

For the $\text{Ca}(\text{BH}_4)_2\text{-CaI}_2$ system iodide is the larger anion and CaI_2 was observed to dissolve significant amounts of the smaller anion BH_4^- , i.e., $\text{Ca}(\text{BH}_4)_2$. Therefore, the initially formed solid solution $\text{tri-Ca}((\text{BH}_4)_{1-x}\text{I}_x)_2$ and CaI_2 are isostructural. The trigonal solid solution $\text{tri-Ca}((\text{BH}_4)_{0.70}\text{I}_{0.30})_2$ transforms at $\sim 180^\circ\text{C}$ to an orthorhombic phase, $\text{ort-Ca}((\text{BH}_4)_{0.64}\text{I}_{0.36})_2$, with a CaCl_2 -type structure (a distorted $\beta\text{-Ca}(\text{BH}_4)_2$ type structure), which may facilitate further dissolution of $\beta\text{-Ca}(\text{BH}_4)_2$ upon heating.

This contrasts the behavior of $\text{LiBH}_4\text{-LiCl}$ system where BH_4^- is the larger anion, and the hexagonal form of LiBH_4 readily dissolve LiCl and stabilize the hexagonal structure to ambient temperatures.³⁵ Notice, that there are no indications of any dissolution of LiBH_4 in the alkali halide salts. Generally, the smaller anion tends to dissolve in the compound containing the larger anion, and the structure of the latter tends to be preserved in the obtained solid solution. This trend follows the relative size of the anions, $\text{I}^- > \text{BH}_4^- > \text{Br}^- > \text{Cl}^-$, derived by a comparison of the unit cell volumes for different inorganic salts.⁶¹ This trend in anion substitution reactions can be interpreted as an increase in the lattice energy due to the clearly observed decrease in the unit cell volume, i.e., a decrease in the average distance between the ions in the structure.

3.3. Thermal Analysis of the New Solid Solutions. Differential scanning calorimetry (DSC) and thermogravimetric analysis (TGA) measurements were conducted for $\text{Ca}(\text{BH}_4)_2\text{-CaI}_2$ samples (S1 and S2) and for $\alpha\text{-Ca}(\text{BH}_4)_2$ (R2) and the data are shown in Figure 11 for the temperature range RT to 500°C (heating rate of $10^\circ\text{C}/\text{min}$). Calcium borohydride decomposes in several steps visible as endothermic peaks at 351 , 379 , and 437°C in the DSC profile. All three peaks are associated with weight loss in accordance with previous reports.^{48,49,68} The first hydrogen release is assigned to the decomposition of $\beta\text{-Ca}(\text{BH}_4)_2$, and the latter to the decomposition of intermediate phases with lower hydrogen contents.⁴⁸ The endothermic peaks

are associated with a total mass loss of $5.46\text{ wt } \%$ in the temperature range from 350 to 400°C , which is less than the calculated gravimetric hydrogen content of $\rho_m = 9.6\text{ wt } \%$, possibly due to insufficient thermal treatment or air exposure.

Two almost coinciding peaks are observed in the DSC-profile for $\text{Ca}(\text{BH}_4)_2\text{-CaI}_2$ (0.82: 0.18, S1), at 384 and 388°C , which supports the SR-PXD results, i.e., formation of $\text{tet-Ca}((\text{BH}_4)_{0.35}\text{I}_{0.65})_2$ (361°C , S1) followed by the decomposition to CaHI , which is observed in the temperature range $330\text{--}400^\circ\text{C}$. The DSC-peaks are related to a total mass loss of $4.0\text{ wt } \%$, which is comparable to the expected gravimetric hydrogen content of $\rho_m = 4.5\text{ wt } \%$ in the sample (see Table 5). On the other hand, a broad endothermic peak is observed at 385°C associated with a mass loss of $2.75\text{ wt } \%$ (calculated gravimetric hydrogen content $\rho_m = 3.13\text{ wt } \%$) for $\text{Ca}(\text{BH}_4)_2\text{-CaI}_2$ (0.71: 0.29, S2). This thermal event may be assigned to the formation of the tetragonal phase and the decomposition to CaHI . The decomposition temperature for samples S1 and S2 are detected at 388 and 385°C , respectively, as compared to 379°C for $\alpha\text{-Ca}(\text{BH}_4)_2$ (R2). Therefore, the anion substitution may have a minor “stabilizing” effect in the range $5\text{--}10^\circ\text{C}$ as compared to $\text{Ca}(\text{BH}_4)_2$. The calculated volumetric and gravimetric hydrogen content of the substituted compounds is shown in the Supporting Information Table s8.

3.4. Hydrogen Release and Uptake in the Solid Solutions $\text{Ca}(\text{BH}_4)_2\text{-CaI}_2$. Sieverts measurements were performed for $\text{Ca}(\text{BH}_4)_2\text{-CaI}_2$ (0.71: 0.29, S2) and for a reference sample of $\alpha\text{-Ca}(\text{BH}_4)_2$ (R2). The desorption measurements were performed in vacuum in the temperature range RT to 550°C ($0.5^\circ\text{C}/\text{min}$) and are shown in Figure 12. The desorption profile of $\alpha\text{-Ca}(\text{BH}_4)_2$, R2, contains at least four different hydrogen release rates starting at 200°C with a maximum just above 300°C . A total hydrogen release of $9.36\text{ wt } \%$ is observed in accordance with the calculated gravimetric hydrogen content of $\rho_m = 9.6\text{ wt } \%$ (see the reaction Scheme 1. After rehydrogenation for 10 h at $T = 350^\circ\text{C}$ and $p(\text{H}_2) = 100\text{ bar}$ a second hydrogen

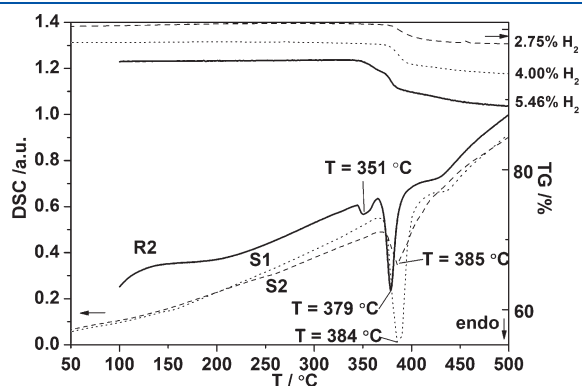


Figure 11. Thermal analysis (DSC and TGA) for $\text{Ca}(\text{BH}_4)_2\text{-CaI}_2$ (0.82: 0.18, S1, dotted line), $\text{Ca}(\text{BH}_4)_2\text{-CaI}_2$ (0.71: 0.29, S2, dashed line) and $\alpha\text{-Ca}(\text{BH}_4)_2$ (R2, solid line). The DSC data are normalized for comparison (heating rate $10^\circ\text{C}/\text{min}$).

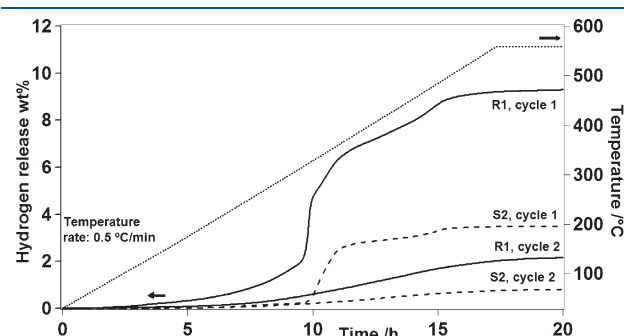


Figure 12. Two cycles of TPD measurements for $\text{Ca}(\text{BH}_4)_2\text{-CaI}_2$ (0.71: 0.29, S2, dashed line) and $\alpha\text{-Ca}(\text{BH}_4)_2$ (R2, solid line) heated from RT to 550°C (heating rate $0.5^\circ\text{C}/\text{min}$) is displayed as hydrogen release (wt %) versus time (h). The temperature profile is displayed as dots, and the temperature scale is shown on the right side of the figure.

Table 5. The Observed and the Calculated Mass Loss (ρ_m) from Samples S1, S2 and R2 Based on Release of Hydrogen

sample	DSC $T_{\text{dec}}/^\circ\text{C}$	TGA obs. mass loss/wt %	PCT cycle 1 obs. mass loss/wt %	PCT cycle 2 obs. mass loss/wt %	$\rho_m(\text{H}_2)/\text{wt } \%$
R2: $\text{Ca}(\text{BH}_4)_2$	379	5.46	9.30	2.16	9.60
S1: $\text{Ca}(\text{BH}_4)_2\text{-CaI}_2$ (0.82: 0.18)	384	4.00			4.50
S2: $\text{Ca}(\text{BH}_4)_2\text{-CaI}_2$ (0.71: 0.29)	385	2.75	3.50	0.81	3.13

desorption is measured for R2 with a release of 2.16 wt % H₂ observed in the temperature range RT to 550 °C, indicating that the sample was not fully loaded with hydrogen using the selected absorption conditions.

For Ca(BH₄)₂–CaI₂ (0.71: 0.29, S2) a relatively fast hydrogen release of 2.20 wt % is observed in the temperature range 320–360 °C followed by another distinct release step at 460 to 500 °C of 0.30 wt % giving a total hydrogen release of 3.50 wt %, which is larger than the calculated gravimetric hydrogen content of the sample of $\rho_m = 3.13$ wt %. The observation of hydrogen release already at 320 °C indicates that the initial hydrogen desorption originates from the *ort*-Ca((BH₄)_{1-x}I_x)₂.

The hydrogen desorption for the substituted sample, S2, occurs at 5–10 °C higher than for the pure α -Ca(BH₄)₂, consistent with the observations from the DSC/TGA. The results from DSC/TGA and from Sieverts measurements compared with the calculated H₂ content are listed in Table 5.

4. CONCLUSION

Anion substitution in the system Ca(BH₄)₂–CaI₂ resulted in the formation of three new compounds, which are solid solutions with BH₄⁻ and I⁻ anions sharing the same positions in the structures. The sample preparation methods have a significant influence on the reaction pathway. Mechano-chemical synthesis (ball milling) mediates a significant degree of dissolution of Ca(BH₄)₂ in CaI₂ (~70%), yielding a CaI₂-type trigonal solid solution, *tri*-Ca((BH₄)_{1-x}I_x)₂ ($x \sim 0.3$). Upon heating, *tri*-Ca((BH₄)_{0.70}I_{0.30})₂ transforms to a CaCl₂-type orthorhombic structure, *ort*-Ca((BH₄)_{1-x}I_x)₂ ($x \sim 0.3$), which is structurally related to β -Ca(BH₄)₂. Upon further heating (at 335 °C), the sample partly transforms to a more iodide-rich tetragonal solid solution, *tet*-Ca((BH₄)_{1-x}I_x)₂ ($x \sim 0.6$, ~20 wt % of sample), with a novel structure type. This compound decomposes to CaHI and CaB₆ (at $T > 345$ °C). The heating of a hand-mixed Ca(BH₄)₂–CaI₂ sample reveals unidentified products and the *tet*-Ca((BH₄)_{1-x}I_x)₂ at $T > 300$ °C. Apparently, minor amounts of CaI₂ dissolve in β -Ca(BH₄)₂ forming a solid solution, which is structurally similar to *ort*-Ca((BH₄)_{1-x}I_x)₂, i.e., β -Ca((BH₄)_{1-x}I_x)₂ ($x \sim 0.05$). Generally, the smaller anion tends to dissolve in the compound containing the larger anion, and the structure of the latter tends to be preserved in the obtained solid solution in accordance with the observation of a CaI₂-type trigonal solid solution, *tri*-Ca((BH₄)_{1-x}I_x)₂. Furthermore, anion substitution can occur when there are structural similarities between the two compounds, which may partly explain the observation of β -Ca((BH₄)_{1-x}I_x)₂ ($x \sim 0.05$). A significant structural diversity is observed within the Ca(BH₄)₂–CaI₂ system, which provides a unique decomposition pathway for the substituted compounds and possibly a minor stabilizing effect.

■ ASSOCIATED CONTENT

Supporting Information. The atomic coordinates and interatomic distances are provided for the three anion substituted solid solutions: *tri*-, *ort*-, and *tet*-Ca((BH₄)_{1-x}I_x)₂. A table showing an overview of the temperature regions where the different compounds are observed in the samples S1–S4 is also provided together with the in situ SR-PXD data for samples S3 and S4. Furthermore, a table with details on physical properties of the three new compounds are available. This material is available free of charge via the Internet at <http://pubs.acs.org>.

■ AUTHOR INFORMATION

Corresponding Author

*E-mail: Yaroslav.Filinchuk@uclouvain.be (Y.F.); Fax: +32 1047 2707; E-mail: trj@chem.au.dk (T.R.J.). Tel: +45 8942 3894. Fax: +45 8619 6199.

■ ACKNOWLEDGMENT

The European Commission (Contract NMP-2008-261/FLYHY) and the Danish Research Council for Natural Sciences (Danscatt) is thanked for financial support. We are grateful to the competent team at the Swiss Norwegian Beam Lines at ESRF for their assistance. The work was also supported by the Danish National Research Foundation (Centre for Materials Crystallography), the Danish Strategic Research Council (Centre for Energy Materials) and the Carlsberg Foundation.

■ REFERENCES

- (1) Ritter, J. A.; Ebner, A. D.; Wang, J.; Zidan, R. *Mater. Today* **2003**, *6*, 18–23.
- (2) Schlapbach, L.; Züttel, A. *Nature* **2001**, *414*, 353–358.
- (3) Felderhoff, M.; Weidenthaler, C.; Helmolt, R.; Eberle, U. *Phys. Chem. Chem. Phys.* **2007**, *9*, 2643–2653.
- (4) U.S. Department of Energy DOE Targets for Onboard Hydrogen Storage Systems for Light-Duty Vehicles. http://www1.eere.energy.gov/hydrogenandfuelcells/storage/pdfs/targets_onboard_hydro_storage.pdf; (accessed March 2011).
- (5) Soloveichik, G. L. *Mater. Matter* **2007**, *2*, 41944.
- (6) Orimo, S.; Nakamori, Y.; Eliseo, J. R.; Züttel, A.; Jensen, C. M. *Chem. Rev.* **2007**, *107*, 4111–4132.
- (7) Grochala, W.; Edwards, P. P. *Chem. Rev.* **2004**, *104*, 1283–1316.
- (8) Filinchuk, Y.; Chernyshov, D.; Dmitriev, V. Z. *Kristallogr.* **2008**, *223*, 649–659.
- (9) Hagemann, H.; Longhini, M.; Kaminski, J. W.; Wesolowski, T. A.; Černý, R.; Penin, N.; Sørby, M. H.; Hauback, B. C.; Severa, G.; Jensen, C. M. *J. Phys. Chem. A* **2008**, *112*, 7551–7555.
- (10) Černý, R.; Severa, G.; Ravnsbæk, D. B.; Filinchuk, Y.; D'Anna, V.; Hagemann, H.; Haase, D.; Jensen, C. M.; Jensen, T. R. *J. Phys. Chem. C* **2010**, *114*, 1357–1364.
- (11) Černý, R.; Ravnsbæk, D. B.; Severa, G.; Filinchuk, Y.; d'Anna, V.; Hagemann, H.; Haase, D.; Skibsted, J.; Jensen, C. M.; Jensen, T. R. *J. Phys. Chem. C* **2010**, *114*, 19540–19549.
- (12) Kim, C.; Hwang, S.; Bowman, R. C.; Reiter, J. W.; Zan, J. A.; Kulleck, J. G.; Kabbour, H.; Majzoub, E. H.; Ozolins, V. *J. Phys. Chem. C* **2009**, *113*, 9956–9968.
- (13) Ravnsbæk, D.; Filinchuk, Y.; Cerenius, Y.; Jakobsen, H. J.; Besenbacher, F.; Skibsted, J.; Jensen, T. R. *Angew. Chem., Int. Ed.* **2009**, *48*, 6659–6663.
- (14) Ravnsbæk, D. B.; Sørensen, L. H.; Filinchuk, Y.; Reed, D.; Book, D.; Jakobsen, H. J.; Besenbacher, F.; Skibsted, J.; Jensen, T. R. *Eur. J. Inorg. Chem.* **2010**, *11*, 1608–1612.
- (15) Jeon, E.; Cho, Y. W. *J. Alloys Compd.* **2006**, *422*, 273–275.
- (16) Kostka, J.; Lohstroh, W.; Fichtner, M.; Hahn, H. J. *J. Phys. Chem. C* **2007**, *111*, 14026–14029.
- (17) Hagemann, H.; D'Anna, V.; Carbonnière, P.; Gil Bardají, E.; Fichtner, M. *J. Phys. Chem. A* **2009**, *113*, 13932–13936.
- (18) Ravnsbæk, D. B.; Filinchuk, Y.; Černý, R.; Ley, M. B.; Haase, D.; Jakobsen, H. J.; Skibsted, J.; Jensen, T. R. *Inorg. Chem.* **2010**, *49*, 3801–3809.
- (19) Frommen, C.; Aliouane, N.; Deledda, S.; Fonnelop, J. E.; Grove, H.; Lieutenant, K.; Llamas-Jansa, I.; Sartori, S.; Sørby, M. H.; Hauback, B. C. *J. Alloys Compd.* **2010**, *496*, 710–716.
- (20) Černý, R.; Penin, N.; Hagemann, H.; Filinchuk, Y. *J. Phys. Chem. C* **2009**, *113*, 9003–9007.

- (21) Filinchuk, Y.; Cerný, R.; Hagemann, H. *Chem. Mater.* **2009**, *21*, 925–933.
- (22) Lee, J. Y.; Ravnsbæk, D.; Lee, Y.; Kim, Y.; Cerenius, Y.; Shim, J.; Jensen, T. R.; Hur, N. H.; Cho, Y. W. *J. Phys. Chem. C* **2009**, *113*, 15080–15086.
- (23) Bösenberg, U.; Doppiu, S.; Mosegaard, L.; Barkhordarian, G.; Eigen, N.; Borgschulte, A.; Jensen, T. R.; Cerenius, Y.; Gutfleisch, O.; Klassen, T.; Dornheim, M.; Bormann, R. *Acta Mater.* **2007**, *55*, 3951–3958.
- (24) Bösenberg, U.; Kim, J. W.; Gosslar, D.; Eigen, N.; Jensen, T. R.; von Colbe, J. M.; Zhou, Y.; Dahms, M.; Kim, D. H.; Günther, R.; Cho, Y. W.; Oh, K. H.; Klassen, T.; Bormann, R.; Dornheim, M. *Acta Mater.* **2010**, *58*, 3381–3389.
- (25) Vajo, J. J.; Skeith, S. L.; Mertens, F. *J. Phys. Chem. B* **2005**, *109*, 3719–3722.
- (26) Cho, Y. W.; Shim, J.; Lee, B. *Calphad* **2006**, *30*, 65–69.
- (27) Yin, L.; Wang, P.; Fang, Z.; Cheng, H. M. *Chem. Phys. Lett.* **2008**, *450*, 318–321.
- (28) Brinks, H. W.; Fossdal, A.; Hauback, B. C. *J. Phys. Chem. C* **2008**, *112*, 5658–5661.
- (29) Kang, X.; Wang, P.; Cheng, H. *Scr. Mater.* **2007**, *56*, 361–364.
- (30) Wang, P.; Kang, X.; Cheng, H. M. *ChemPhysChem* **2005**, *6*, 2488–2491.
- (31) Eigen, N.; Bösenberg, U.; Bellosta von Colbe, J.; Jensen, T. R.; Cerenius, Y.; Dornheim, M.; Klassen, T.; Bormann, R. *J. Alloys Compd.* **2009**, *477*, 76–80.
- (32) Hauback, B. C. *Z. Kristallogr.* **2008**, *223*, 636–648.
- (33) Maekawa, H.; Matsuo, M.; Takamura, H.; Ando, M.; Noda, Y.; Karahashi, T.; Orimo, S. *J. Am. Chem. Soc.* **2009**, *131*, 894–895.
- (34) Mosegaard, L.; Möller, B.; Jørgensen, J.; Filinchuk, Y.; Cerenius, Y.; Hanson, J. C.; Dimasi, E.; Besenbacher, F.; Jensen, T. R. *J. Phys. Chem. C* **2008**, *112*, 1299–1303.
- (35) Arnbjerg, L. M.; Ravnsbæk, D. B.; Filinchuk, Y.; Vang, R. T.; Cerenius, Y.; Besenbacher, F.; Jørgensen, J.; Jakobsen, H. J.; Jensen, T. R. *Chem. Mater.* **2009**, *21*, 5772–5782.
- (36) Lee, J. Y.; Lee, Y.; Suh, J.; Shim, J.; Cho, Y. W. *J. Alloys Compd.* **2010**, *506*, 721–727.
- (37) Rönnebro, E.; Majzoub, E. H. *J. Phys. Chem. B* **2007**, *111*, 12045–12047.
- (38) Miwa, K.; Aoki, M.; Noritake, T.; Ohba, N.; Nakamori, Y.; Towata, S.; Züttel, A.; Orimo, S. *Phys. Rev. B* **2006**, *74*, 155122.
- (39) Kim, J.; Jin, S.; Shim, J.; Cho, Y. W. *Scr. Mater.* **2008**, *58*, 481–483.
- (40) Filinchuk, Y.; Rönnebro, E.; Chandra, D. *Acta Mater.* **2009**, *57*, 732–738.
- (41) Buchter, F.; Łodziana, Z.; Remhof, A.; Friedrichs, O.; Borgschulte, A.; Mauron, P.; Züttel, A.; Sheptyakov, D.; Barkhordarian, G.; Bormann, R.; Chłopek, K.; Fichtner, M.; Sørby, M.; Riktor, M.; Hauback, B.; Orimo, S. *J. Phys. Chem. B* **2008**, *112*, 8042–8048.
- (42) Aoki, M.; Miwa, K.; Noritake, T.; Ohba, N.; Matsumoto, M.; Li, H.; Nakamori, Y.; Towata, S.; Orimo, S. *Appl. Phys. A: Mater. Sci. Process.* **2008**, *92*, 601–605.
- (43) Barkhordarian, G.; Jensen, T. R.; Doppiu, S.; Bösenberg, U.; Borgschulte, A.; Gremaud, R.; Cerenius, Y.; Dornheim, M.; Klassen, T.; Bormann, R. *J. Phys. Chem. C* **2008**, *112*, 2743–2749.
- (44) Lee, Y.; Kim, Y.; Cho, Y.; Shapiro, D.; Wolverton, C.; Ozoliņš, V. *Phys. Rev. B* **2009**, *79*.
- (45) Buchter, F.; Łodziana, Z.; Remhof, A.; Friedrichs, O.; Borgschulte, A.; Mauron, P.; Züttel, A.; Sheptyakov, D.; Palatinus, L.; Chłopek, K.; Fichtner, M.; Barkhordarian, G.; Bormann, R.; Hauback, B. C. *J. Phys. Chem. C* **2009**, *113*, 17223–17230.
- (46) Noritake, T.; Aoki, M.; Matsumoto, M.; Miwa, K.; Towata, S.; Li, H.; Orimo, S. *J. Alloys Compd.* **2010**, *491*, 57–62.
- (47) Fichtner, M.; Chłopek, K.; Longhini, M.; Hagemann, H. *J. Phys. Chem. C* **2008**, *112*, 11575–11579.
- (48) Riktor, M. D.; Sørby, M. H.; Chłopek, K.; Fichtner, M.; Buchter, F.; Züttel, A.; Hauback, B. C. *J. Mater. Chem.* **2007**, *17*, 4939–4942.
- (49) Kim, Y.; Reed, D.; Lee, Y.; Lee, J. Y.; Shim, J.; Book, D.; Cho, Y. W. *J. Phys. Chem. C* **2009**, *113*, 5865–5871.
- (50) Kim, J.; Shim, J.; Cho, Y. W. *J. Power Sources* **2008**, *181*, 140–143.
- (51) Jensen, T. R.; Nielsen, T. K.; Filinchuk, Y.; Jørgensen, J. E.; Cerenius, Y.; Gray, E. M.; Webb, C. J. *J. Appl. Crystallogr.* **2010**, *43*, 1456–1463.
- (52) Hammersley, A. P.; Svensson, S. O.; Hanfland, M.; Fitch, A. N.; Hausermann, D. *High Pressure Res.* **1996**, *14*, 235–248.
- (53) Vogel, S.; Ehm, L.; Knorr, K.; Braun, C. *Adv. X-ray Anal.* **2002**, *45*, 31–33.
- (54) Boultaf, A.; Louër, D. *J. Appl. Crystallogr.* **2004**, *37*, 724–731.
- (55) Favre-Nicolin, V.; Cerný, R. *J. Appl. Crystallogr.* **2002**, *35*, 734–743.
- (56) Rodriguez-Carvajal, J. *FullProf Suite*; LLB Sacley & LCSIM: Rennes, France, 2003.
- (57) Blum, H. Z. *Phys. Chem. B* **1933**, *22*, 298–304.
- (58) Ehrlich, P.; Kulke, H. Z. *Anorg. Allg. Chem.* **1956**, *288*, 156–170.
- (59) Busing, W. R. *Trans. Am. Cryst. Assoc.* **1970**, *6*, 57–72.
- (60) PCTPro-2000 - Calorimetry and thermal analysis, <http://www.setaram.com/PCTPro-2000.htm>; (accessed March 2011).
- (61) Filinchuk, Y.; Hagemann, H. *Eur. J. Inorg. Chem.* **2008**, *20*, 3127–3133.
- (62) Howard, C. J.; Kennedy, B. J.; Curfs, C. *Phys. Rev. B* **2005**, *72*, 214114.
- (63) Brostigen, G.; Kjekshus, A. *Acta Chem. Scand.* **1970**, *24*, 1925–1940.
- (64) Abrahams, S. C.; Schmalle, H. W.; Williams, T.; Reller, A.; Lichtenberg, F.; Widmer, D.; Bednorz, J. G.; Spreiter, R.; Bosshard, C.; Günter, P. *Acta Crystallogr. B: Struct. Sci.* **1998**, *54*, 399–416.
- (65) Filinchuk, Y.; Chernyshov, D.; Nevidomskyy, A.; Dmitriev, V. *Angew. Chem., Int. Ed.* **2008**, *47*, 529–532.
- (66) Majzoub, E. H.; Rönnebro, E. *J. Phys. Chem. C* **2009**, *113*, 3352–3358.
- (67) Balema, V. P. *Mater. Matter* **2007**, *2*, 16–18.
- (68) Kim, J.; Jin, S.; Shim, J.; Cho, Y. W. *J. Alloys Compd.* **2008**, *461*, L20–L22.